

Hamiltonian dynamics generated by Vassiliev invariants

Mitchell A Berger

Mathematics, University College London, Gower Street, London WC1E 6BT, UK

E-mail: m.berger@ucl.ac.uk

Received 6 September 2000

Abstract

This paper employs higher-order winding numbers to generate Hamiltonian motion of particles in two dimensions. The ordinary winding number counts how many times two particles rotate about each other. Higher-order winding numbers measure braiding motions of three or more particles. These winding numbers relate to various invariants known in topology and knot theory, for example Massey and Milnor numbers, and can be derived from Vassiliev–Kontsevich integrals. The invariants can be regarded as complex-valued functions of the paths of the particles. The real part gives the winding number, whereas the imaginary part seems uninteresting.

In this paper, we set the imaginary part to be a Hamiltonian for particle motions. For just two particles, this gives the familiar motion of two point vortices. However, for three or more particles, the Hamiltonian generates more complicated intertwining patterns. We examine the dynamics for the case of three particles, and show that the motion is completely integrable. The intertwining patterns correspond to periodic braids; closure of these braids gives links such as the Borromean rings. The Hamiltonian provides an elegant method for generating simple geometrical examples of complicated braids and links.

PACS numbers: 0210K, 4505, 4520J

(Some figures in this article are in colour only in the electronic version; see www.iop.org)

1. Introduction

Topological invariants have been an essential tool in the study of knots and links. This paper shows how a particular set of invariants can be used to generate interesting dynamics. In particular, we will employ higher-order winding numbers from braid theory as Hamiltonians for particle motion in a plane.

A geometrical braid is a set of curves stretching between two parallel planes. Two braids can be considered topologically equivalent if one can be deformed into the other by smooth

motions vanishing at the boundary planes. A topological braid consists of an equivalence class of geometrical braids. If t denotes the vertical direction, then N braided curves can be described by functions $(x_i(t), y_i(t))$, $i = 1, \dots, N$. If t represents time rather than a third spatial direction, then the braid gives us a spacetime diagram of N particles moving in a plane. In other words, if we look at the motion for some fixed time T then the braid records a history of the motion for $0 < t < T$. Braided spacetime diagrams provide a valuable tool for two-dimensional dynamics [1–3]. In the time period $0 < t < T$ two particles labelled i and j will rotate about each other through some angle $\theta_{ij}(T)$. The winding number $\theta_{ij}(T)/2\pi$ gives the net number of complete turns. All topologically equivalent braids will have the same set of winding numbers. Winding numbers are closely related to linking numbers. For example, if the braid is periodic, so that $(x_i(0), y_i(0)) = (x_i(T), y_i(T))$, then we can join up the endpoints to form closed curves (e.g. by embedding the braid in the interior of a torus). In this process the winding numbers become Gauss linking numbers.

The Gauss linking number (for historical details, see [9]) does not detect all forms of linking. For example, the Borromean rings [10] (see figure 5 below) cannot be pulled apart, and yet have zero Gauss linking number between any pair of rings. In the early 1950s, higher-order linking numbers were discovered by Massey and Milnor. These were later shown to be equivalent by the Porter–Turaev theorem (see [11] for a comprehensive review). Gauss linking numbers can be studied in the context of physical vector fields such as magnetism and vorticity [12–15]. Similarly, the higher-order linking numbers can be expressed using vector fields [16–21]. This makes aspects of knot theory more widely available for use in the physical and applied sciences.

In 1991, a higher-order winding number was devised for three-braids [22, 23]. For closed braids, this number reproduced the Massey–Milnor numbers. The three-braid invariant provides the principal ingredient for constructing the Hamiltonian system described in this paper.

In 1990 Vassiliev [4] discovered a powerful tool for analysing knot invariants by considering their extension to curves with double points (i.e. points where a curve intersects itself). Suppose a knotted curve has n double points. We can remove one of the double points by turning it into an overcrossing or an undercrossing. Suppose we can calculate an invariant I_{n-1} defined for curves with $n-1$ double points. Then this invariant can be extended to a new invariant I_n defined for curves with n double points in the following way: remove one of the n double points by changing it into an overcrossing or an undercrossing. For either of these choices of crossing, I_{n-1} can be calculated. Now take their difference: $I_n = I_{n-1}^+ - I_{n-1}^-$ where I_{n-1}^+ is the calculated invariant for the overcrossing. Note that the usual knot, link, or braid invariants are for curves with zero double points, so they are of the form I_0 . Two I_0 numbers must be calculated (and their difference taken) to calculate an I_1 invariant. Similarly two I_1 numbers, and hence four I_0 numbers, determine an I_2 invariant. Thus in general 2^n I_0 numbers determine an I_n .

There may not be an infinite series of invariants I_0, I_1, \dots , however. A finite-type invariant (now known as a Vassiliev invariant) of order m vanishes for more than m double points, i.e. $I_m \neq 0$ (for some curve), but $I_{m+1} = I_{m+2} = \dots = 0$ (for all curves) [5]. The Gauss linking number is an order one invariant. Many famous knot invariants such as the Jones polynomial are also Vassiliev invariants. In 1993 Kontsevich [6] showed that Vassiliev invariants can be found using an integral formula. In practice, Kontsevich integrals can often be difficult to calculate, as they involve many terms and require working with special diagrams called chord diagrams [7]. However, they have provided knot theorists with valuable information about the general structure of invariants (for a bibliography on Vassiliev–Kontsevich theory, see [8]). Recently, Willerton [24] showed that the higher-order winding number for three-braids is a

finite-type (order two) Vassiliev invariant, and showed how to obtain it from the Kontsevich integral. He also obtained expressions for similar invariants of higher order.

Section 2 reviews the use of complex coordinates for Hamiltonian variables. As we construct our Hamiltonians from the imaginary part of analytic functions (more precisely, analytic on Riemann surfaces), complex coordinates are essential. This section proves a simple theorem, that the Hamiltonian flow follows the gradient of the real part of the analytic function. The real part supplies the topological data.

Section 3 reviews the Hamiltonian for point vortex motion. This Hamiltonian can be expressed using the complex logarithm. When this logarithm is extended to a Riemann surface above the complex plane, it includes the winding number of two vortices as they orbit each other. Winding number is a first-order Vassiliev invariant.

Second-order three-braid invariants are described in section 4. Symmetries, conservation laws and integrability of the Hamiltonians derived from these invariants will be discussed. Conclusions are given in section 5.

It may be useful here to emphasize the distinction between *dynamical invariants* and *topological invariants* when applied to particle motions. A dynamical invariant is a function f of the particle positions and velocities which is conserved, $df/dt = 0$. On the other hand, a topological invariant $\Psi(T)$ is a quantity calculated from the braided spacetime diagram of the particle motion between $t = 0$ and T . Distortions of the braid (away from the Hamiltonian solution) keeping fixed endpoints at $t = 0, T$ do not change $\Psi(T)$, hence the term ‘invariant’. However, at a slightly later time $T + \delta T$ the Hamiltonian solution will have a slightly different spacetime diagram, because of the motion during the time δT . Thus $\Psi(T + \delta T) \neq \Psi(T)$ in general. In other words, $d\Psi(T)/dT \neq 0$. Perhaps ‘topological quantity’ may be a more appropriate term for Ψ , as it measures aspects of topological structure which do indeed change with time.

2. Hamiltonian theory with complex coordinates

Suppose we have an analytic function $F(z)$, or more generally $F(z_1, \dots, z_n)$ analytic in n complex variables. What happens if we use the real part of F as a Hamiltonian? As we will be doing this below, we set the scene by first reviewing complex coordinates, then discuss Hamiltonians derived from analytic functions.

2.1. Review of complex coordinates

Consider first a one-dimensional Hamiltonian system with coordinate x and its conjugate momentum p . Let $z = (x + ip)$. The so-called Wirtinger calculus uses a complex number z and its complex conjugate \bar{z} as independent variables. In particular, with variables (z, \bar{z}) the basis one-forms are

$$dz = (dx + i dp) \quad d\bar{z} = (dx - i dp). \quad (1)$$

The basis vectors dual to these are

$$\partial_z = \frac{1}{2}(\partial_x - i\partial_p) \quad \partial_{\bar{z}} = \frac{1}{2}(\partial_x + i\partial_p). \quad (2)$$

Note that

$$\frac{\partial z}{\partial \bar{z}} = \frac{\partial \bar{z}}{\partial z} = 0. \quad (3)$$

Recall that the time-derivative of a function $f(x, p)$ induced by the particle motion is given by the Poisson bracket of f with the Hamiltonian H , $df/dt = [f, H]$, where

$$[f, g] \equiv \frac{\partial f}{\partial x} \frac{\partial g}{\partial p} - \frac{\partial f}{\partial p} \frac{\partial g}{\partial x}. \quad (4)$$

In complex coordinates, let

$$\{f, g\} \equiv \partial_z f \partial_{\bar{z}} g - \partial_{\bar{z}} f \partial_z g. \quad (5)$$

A simple calculation gives $[f, g] = -2i\{f, g\}$, so

$$\frac{df}{dt} = -2i\{f, H\}. \quad (6)$$

For a Hamiltonian function of several variables (x_1, \dots, x_n) with conjugate momenta (p_1, \dots, p_n) , we let $z_j = x_j + ip_j$. Let $\partial_j \equiv \partial_{z_j}$, $\bar{\partial}_j \equiv \partial_{\bar{z}_j}$. The Poisson brackets become

$$[f, g] \equiv \sum_{j=1}^n \frac{\partial f}{\partial x_j} \frac{\partial g}{\partial p_j} - \frac{\partial f}{\partial p_j} \frac{\partial g}{\partial x_j} \quad (7)$$

$$\{f, g\} \equiv \sum_{j=1}^n \partial_j f \bar{\partial}_j g - \bar{\partial}_j f \partial_j g. \quad (8)$$

2.2. Hamiltonians derived from analytic functions

Suppose that we have an analytic function $F(z_1, \dots, z_n)$. An interesting thing happens when we use its imaginary part as a Hamiltonian. In particular, let

$$F = K + iH \quad (9)$$

where both H and K are real. From equation (6),

$$\frac{dz_j}{dt} = -2i\{z_j, H\} = -\{z_j, F - \bar{F}\}. \quad (10)$$

Thus Hamilton's equations become

$$\frac{dz_j}{dt} = \bar{\partial}_j \bar{F}. \quad (11)$$

Hamiltonian motion, of course, preserves the Hamiltonian itself; i.e. $dH/dt = 0$. What about K ? After all, since F is analytic in each of its variables K must be related to H by the Cauchy–Riemann equations. In fact, the motion maximizes the growth of K . To see this, we calculate the gradient of K and convert it to a vector using the Euclidean metric. This vector turns out to be the same as the velocity vector of the Hamiltonian motion.

Let the metric line element be $ds^2 = ds_1^2 + ds_2^2 + \dots + ds_n^2$ where

$$ds_j^2 = dx_j^2 + dp_j^2 = dz_j d\bar{z}_j. \quad (12)$$

In complex coordinates the Euclidean metric is block-diagonal with matrices

$$g_{j\alpha\beta} = \frac{1}{2} \begin{pmatrix} 0 & 1 \\ 1 & 0 \end{pmatrix}. \quad (13)$$

Also, in complex coordinates

$$\nabla_j K = \begin{pmatrix} \partial_j K \\ \bar{\partial}_j K \end{pmatrix}. \quad (14)$$

If we employ the inverse metric as a raising operator, then we obtain

$$\nabla_j^\alpha K = g_j^{\alpha\beta} \nabla_{j\beta} K = 2 \begin{pmatrix} \bar{\partial}_j K \\ \partial_j K \end{pmatrix} = \begin{pmatrix} \bar{\partial}_j \bar{F} \\ \partial_j F \end{pmatrix}. \quad (15)$$

On the other hand, if we define

$$\mathcal{Z}_j = \begin{pmatrix} z_j \\ \bar{z}_j \end{pmatrix} \tag{16}$$

then

$$\frac{d\mathcal{Z}_j}{dt} = \begin{pmatrix} \bar{\partial}_j \bar{F} \\ \partial_j F \end{pmatrix} = \nabla_j^\alpha K. \tag{17}$$

In effect, the Hamiltonian flow travels along the gradient of K .

In the sections that follow, the functions F will be functions derivable from the Vassiliev–Kontsevich integral, where the real part K gives a topological invariant.

3. Two-particle vortex motion

Before considering higher-order winding numbers, we first review Hamiltonians based on the ordinary two-particle winding number. Consider two point vortices a and b at positions (a_x, a_y) and (b_x, b_y) . (A review of the point vortex problem appears in [25].) For point vortex motion, the x and y coordinates are conjugate to each other: for example the conjugate momentum to a_x is a_y . The Hamiltonian for vortices of equal (unit) vorticity is

$$H = -\frac{1}{2\pi} \log r_{ab} \tag{18}$$

where $r_{ab} = a - b$. The corresponding Lagrangian is (using a dot to denote the time derivative)

$$\mathcal{L} = \frac{1}{2\pi} \log r_{ab} + (\dot{a}_x a_y - a_x \dot{a}_y) + (\dot{b}_x b_y - b_x \dot{b}_y). \tag{19}$$

Hamilton’s equations give

$$(\dot{a}_x, \dot{a}_y) = \left(\frac{\partial H}{\partial a_y}, -\frac{\partial H}{\partial a_x} \right) = \frac{1}{2\pi} \left(-\frac{a_y - b_y}{r_{ab}^2}, \frac{a_x - b_x}{r_{ab}^2} \right) \tag{20}$$

$$(\dot{b}_x, \dot{b}_y) = \left(\frac{\partial H}{\partial b_y}, -\frac{\partial H}{\partial b_x} \right) = \frac{1}{2\pi} \left(-\frac{b_y - a_y}{r_{ab}^2}, \frac{b_x - a_x}{r_{ab}^2} \right). \tag{21}$$

The two vortices rotate about each other at constant radius; the motion maximizes the growth of winding number.

As in the previous section, the Hamiltonian is just the real part of an interesting complex function. Let us extend the logarithm from its principal part to something that lives on a helical Riemann surface. Define

$$\lambda_{ab}(t) \equiv \frac{1}{2\pi i} \int_0^t \frac{\dot{a} - \dot{b}}{a - b} dt'. \tag{22}$$

Then

$$H = \text{Im}(\lambda_{ab}) \tag{23}$$

and

$$\dot{a} = \bar{\partial}_a \bar{\lambda}_{ab} \quad \dot{b} = \bar{\partial}_b \bar{\lambda}_{ab}. \tag{24}$$

Suppose we make a spacetime diagram of the two points, with t the vertical direction extending from $t = 0$ to some final time $t = T$. We obtain a simple braid diagram. The real part of λ_{ab} records how many times the points have circled each other. In fact, λ_{ab} is a topological invariant of braids. Here the invariance is not in *time*, but to deformations of the braid which leave endpoints at $t = 0, T$ fixed.

The topological invariance arises from an application of Stoke’s theorem. If we were to deform the braid from, say, braid configuration 1 to braid configuration 2, then we would change $\lambda_{ab}(T)$ by

$$\lambda_{ab2}(T) - \lambda_{ab1}(T) = \frac{1}{2\pi i} \int_1 \frac{\dot{a} - \dot{b}}{a - b} dt' - \frac{1}{2\pi i} \int_2 \frac{\dot{a} - \dot{b}}{a - b} dt'. \tag{25}$$

This can be regarded as a single integral over a closed path γ in $\mathbb{C} \times \mathbb{C}$, where each point on the path gives the positions of a and b at some time t . Thus

$$\lambda_{ab2}(T) - \lambda_{ab1}(T) = \oint_{\gamma} \omega_{ab} \tag{26}$$

where

$$\omega_{ab} = \frac{1}{2\pi i} \frac{da - db}{a - b}. \tag{27}$$

The closed path γ bounds a region in $\mathbb{C} \times \mathbb{C}$. Applying Stoke’s theorem turns the line integral into a surface integral over this region, of the two-form $d\omega$. However, ω is *closed* ($d\omega_{ab} = 0$), therefore $\lambda_{ab2}(T) = \lambda_{ab1}(T)$.

In cohomology theory topological invariants arise whenever you have a form like ω_{ab} which is closed but not *exact* (not the exterior derivative of a well behaved potential). A closed form which is exact just integrates to give the values of its potential at the boundaries, which is often less interesting. Note that ω_{ab} looks like $d\lambda_{ab}$; however λ_{ab} is not well behaved, being multi-valued.

4. Three-particle Hamiltonian

4.1. Equations of motion

Consider three points a, b and c moving in \mathbb{C} . We assume that the points avoid each other; i.e., $a \neq b, a \neq c, c \neq a$. Let $\tilde{\lambda}_{ab}(t) = \lambda_{ab}(t) + \lambda_{ab0}$ where λ_{ab0} is a constant (for example, λ_{ab0} could be chosen as the principal value of $\log(b(0) - a(0))$). The one-form

$$\psi_{abc} \equiv \frac{1}{2}((\tilde{\lambda}_{ab} - \tilde{\lambda}_{bc}) d\tilde{\lambda}_{ca} + (\tilde{\lambda}_{bc} - \tilde{\lambda}_{ca}) d\tilde{\lambda}_{ab} + (\tilde{\lambda}_{ca} - \tilde{\lambda}_{ab}) d\tilde{\lambda}_{bc}) \tag{28}$$

is the analogy of ω above, and satisfies [22]

$$d\psi_{abc} = 0 \tag{29}$$

so ψ is also closed but not exact. The real part of the integral

$$\Psi_{abc}(T) = \int_0^T \psi_{abc}(t) \tag{30}$$

provides a second-order Vassiliev invariant associated with Massey numbers [19, 22, 24]. In analogy with the previous section, we construct a Hamiltonian $H = \text{Im } \Psi$. From (11),

$$\dot{a} = \bar{\partial}_a \bar{\Psi}_{abc} \quad \dot{b} = \bar{\partial}_b \bar{\Psi}_{abc} \quad \dot{c} = \bar{\partial}_c \bar{\Psi}_{abc}. \tag{31}$$

For example,

$$\dot{a} = -\frac{1}{2} \left((\bar{\lambda}_{ab} - \bar{\lambda}_{bc}) \frac{\partial \bar{\lambda}_{ca}}{\partial \bar{a}} + (\bar{\lambda}_{bc} - \bar{\lambda}_{ca}) \frac{\partial \bar{\lambda}_{ab}}{\partial \bar{a}} + (\bar{\lambda}_{ca} - \bar{\lambda}_{ab}) \frac{\partial \bar{\lambda}_{bc}}{\partial \bar{a}} \right) \tag{32}$$

$$= \frac{1}{4\pi i} \left((\bar{\lambda}_{ab} - \bar{\lambda}_{bc}) \frac{1}{\bar{a} - \bar{c}} - (\bar{\lambda}_{bc} - \bar{\lambda}_{ca}) \frac{1}{\bar{a} - \bar{b}} \right). \tag{33}$$

It will be convenient to define

$$\xi \equiv \frac{1}{4\pi i} \left(\frac{(a-b)\tilde{\lambda}_{ab} + (b-c)\tilde{\lambda}_{bc} + (c-a)\tilde{\lambda}_{ca}}{(a-b)(b-c)(c-a)} \right). \tag{34}$$

The time derivatives become

$$\begin{aligned} \dot{a} &= (\bar{b} - \bar{c})\bar{\xi} \\ \dot{b} &= (\bar{c} - \bar{a})\bar{\xi} \\ \dot{c} &= (\bar{a} - \bar{b})\bar{\xi}. \end{aligned} \tag{35}$$

4.2. Constants of motion

Equation (35) immediately gives a constant centre of mass m (zero linear momentum):

$$\frac{d}{dt}(a + b + c) = \frac{dm}{dt} = 0. \tag{36}$$

The conservation of centre of mass arises, via Noether’s theorem, from the invariance of Ψ_{abc} to translations. Secondly,

$$\bar{a}\dot{a} + \bar{b}\dot{b} + \bar{c}\dot{c} = 0. \tag{37}$$

The real part of this equation gives

$$\frac{d}{dt}(|a|^2 + |b|^2 + |c|^2) = 0. \tag{38}$$

The imaginary part gives zero net angular momentum. To see this note that if $z = re^{i\theta}$ is a complex number,

$$\bar{z}\dot{z} = r\dot{r} + ir^2\dot{\theta}. \tag{39}$$

These conservation laws arise from the scaling and rotational symmetries of Ψ_{abc} .

We can also form a conserved quantity from relative positions. Equation (35) gives

$$\begin{aligned} \dot{a} - \dot{b} &= -3(\bar{c} - m/3)\bar{\xi} \\ \dot{b} - \dot{c} &= -3(\bar{a} - m/3)\bar{\xi} \\ \dot{c} - \dot{a} &= -3(\bar{b} - m/3)\bar{\xi}. \end{aligned} \tag{40}$$

Dot with $(\bar{a} - \bar{b}, \bar{b} - \bar{c}, \bar{c} - \bar{a})$:

$$(\bar{a} - \bar{b})(\dot{a} - \dot{b}) + (\bar{b} - \bar{c})(\dot{b} - \dot{c}) + (\bar{c} - \bar{a})(\dot{c} - \dot{a}) = 0. \tag{41}$$

This gives equations analogous to (38) and (39) in the relative coordinates $(a - b, b - c, c - a)$.

We really only need two relative coordinates, say $(a - b)$ and $(b - c)$, as well as the centre of mass m , which is ignorable. Thus the translational symmetry brings the Hamiltonian system down to two dimensions. The scaling-rotational symmetry gives a new conservation law (41). For a two-dimensional system, the existence of a conserved quantity guarantees complete integrability.

4.3. Winding number diagrams

Define a phase space or winding number space as in [22,23], which consists of the set of triplets $(\text{Re } \tilde{\lambda}_{ab}, \text{Re } \tilde{\lambda}_{bc}, \text{Re } \tilde{\lambda}_{ca})$ (see figure 1). As the points $a(t)$, $b(t)$ and $c(t)$ move according to the dynamics, a single point $\text{Re}(\tilde{\lambda}_{ab}(t), \tilde{\lambda}_{bc}(t), \tilde{\lambda}_{ca}(t))$ will traverse a path in the winding number space (see figure 1). The three axes in the figure correspond to the three winding numbers; the triangular regions shown form part of a plane $\mathcal{P} = \{\text{Re}(\tilde{\lambda}_{ab} + \tilde{\lambda}_{bc} + \tilde{\lambda}_{ca}) = 0\}$.

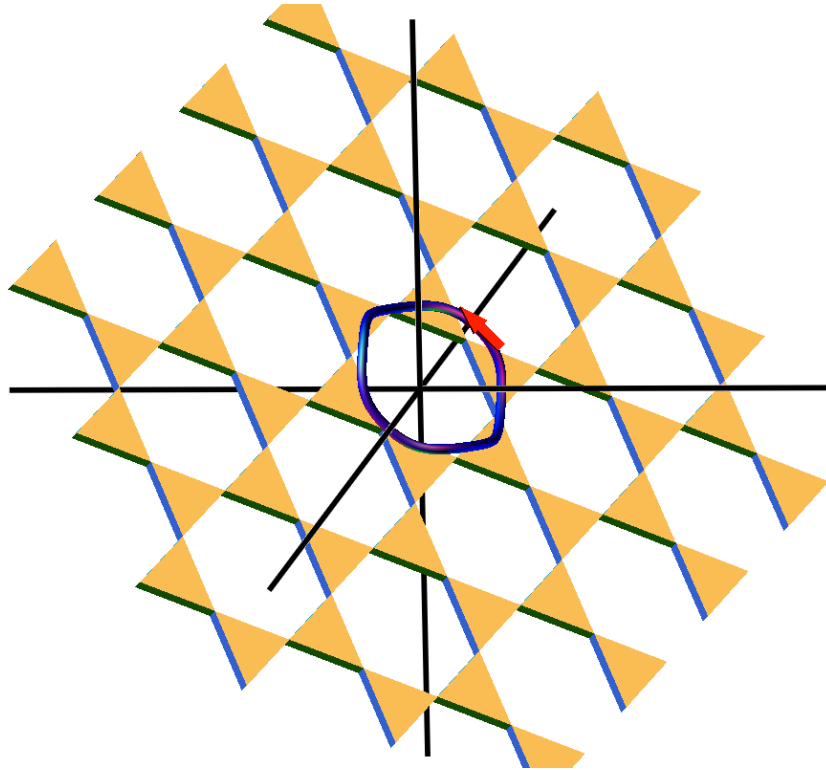


Figure 1. Space of winding numbers $(\operatorname{Re} \tilde{\lambda}_{ab}, \operatorname{Re} \tilde{\lambda}_{bc}, \operatorname{Re} \tilde{\lambda}_{ca})$. The plane $\mathcal{P} = \operatorname{Re}(\tilde{\lambda}_{ab} + \tilde{\lambda}_{bc} + \tilde{\lambda}_{ca}) = 0$ is shown within this space. Hexagonal regions are forbidden. A path is also shown, corresponding to the pigtail braid of figure 2.

The direction perpendicular to this plane corresponds to all three angles increasing at once, i.e. uniform rotation of a , b and c . The white triangular regions correspond to physically accessible combinations of angles. In between are hexagonal regions; a point inside one of these regions corresponds to an impossible set of angles. Vertices of the triangles correspond to a , b and c being collinear. The phase point reaches the centre of a triangular region in \mathcal{P} when a , b and c form an equilateral triangle in \mathbb{C} . Note that there are infinitely many copies of the triangular regions, corresponding to winding angles greater than 2π , i.e. different branches of the complex logarithms.

4.4. Numerical experiments

We use a fourth-order Runge–Kutta code to follow the Hamiltonian motion according to (35). The initial positions of the points a , b and c are set so that they are collinear, with b in the middle. Let ρ denote the initial ratio of distances $\rho = |b - a|/|c - b|$. Thus the initial positions in the complex plane can be classified according to the single parameter ρ . However, the Hamiltonian is a function on a Riemann surface above the complex plane, rather than the complex plane alone thus, to calculate the complex number ξ which appears in (35), we need to specify the initial values of the winding angles.

For the motion shown in figure 2, we set $\rho = 1$, and $\operatorname{Re} \lambda_{ab0} = \operatorname{Re} \lambda_{bc0} = 0$, $\operatorname{Re} \lambda_{ca0} = 1/2$. We plot the result as a spacetime braid diagram (figure 2), and also as a

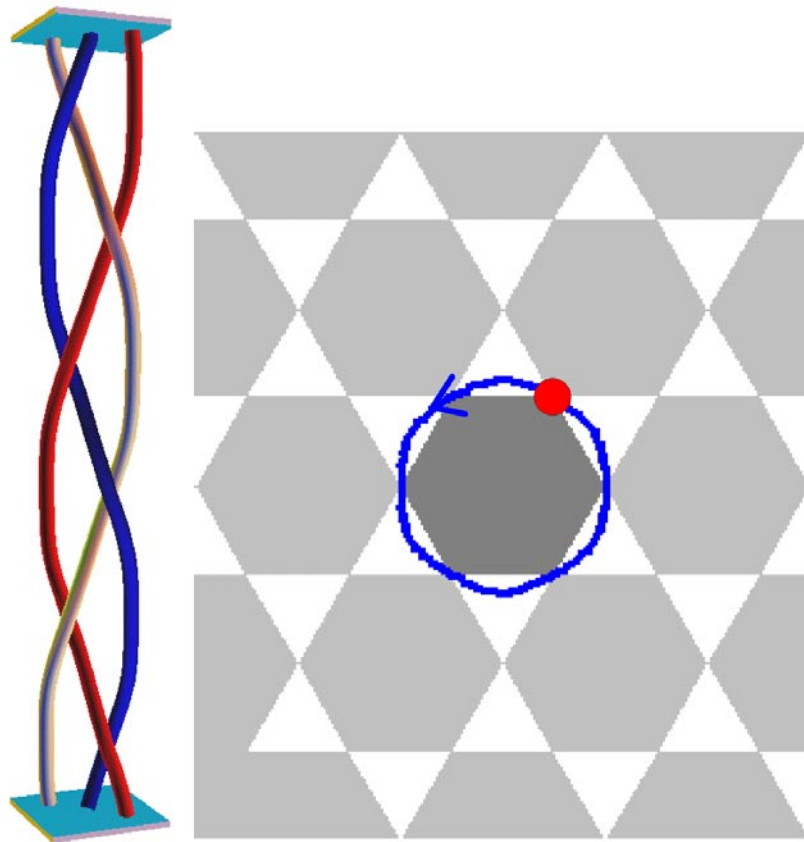


Figure 2. Braid and winding diagram for $\rho = 1$. The initial position (a, b and c collinear with b in the middle) is shown by the dot in the winding diagram. The net rotation $W(P)$ of this braid is zero.

path in the winding plane \mathcal{P} . The motion is periodic. Within a period P the braid acquires exactly one unit of higher-order winding number, i.e. $\text{Re } \Psi_{abc}(P) = 1$. Note that the winding space path encircles precisely one forbidden hexagon, in an anti-clockwise sense. In fact, for any closed curve in \mathcal{P} , Ψ_{abc} equals the number of hexagons encircled anti-clockwise minus the number encircled clockwise [22]. Recall that the winding plane \mathcal{P} projects out the uniform rotation $W = \text{Re}(\lambda_{ab} + \lambda_{bc} + \lambda_{ca})$. While the motion has zero angular momentum (see equations (37) and (39)), W can nevertheless change in time. For this braid with $\rho = 1$, however, we find $W(P) = 0$.

When we vary ρ away from unity, the braid geometry becomes more and more distorted. However, the experiments show that the topology of the braid remains the same (except for a uniform rotation: $W(P) \neq 0$) until $\rho \approx 4.3$, where it jumps to a new pattern, as shown in figure 3.

We can also generate interesting braids by changing the initial branch of the logarithms. Figure 4 shows a braid with $\rho = 1$ (equal intervals between points), but with an extra unit of winding in $\text{Re } \lambda_{ca0}$.

Finally, we note that the closure of a braid becomes a knot or link. We do this graphically by mapping the central vertical axis of the braid ($x, y) = 0$ onto a circle; the x direction maps to

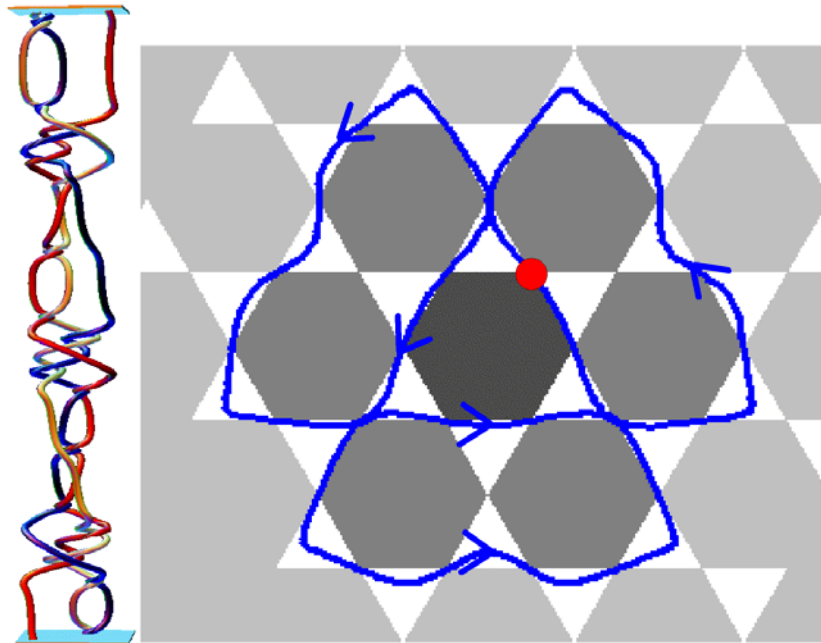


Figure 3. Braid and winding diagram for $\rho = 4.3$. For this braid, $\text{Re } \Psi_{abc}(P) = 8$.

the normal direction of the circle, while the y direction maps to the binormal. If $W(P) \neq 2n\pi$, then a rotation would also need to be included. This is not the case for the braids of figures 2 and 4; links associated with these braids are shown in figure 5. Both of these are examples of Brunnian links, where lower-order winding numbers (e.g. $\lambda_{ab}(P)$) all vanish.

5. Conclusions

Usually topological invariants are calculated for a pre-existing object such as a knot or braid. Here this process is reversed: the topological invariant generates the object. In particular, braid invariants can be employed as Hamiltonians for particles moving in two dimensions. Spacetime diagrams of the particle motions display highly braided patterns which optimize the associated topological invariant (i.e. the Hamiltonian suppresses wasted motions perpendicular to the gradient of the invariant). We have investigated the Hamiltonian for three-particle motion in some detail, and have shown it to be completely integrable.

This paper may be contrasted with other methods of generating the geometry of a knot or braid. For example, minimizing an energy functional [26, 27], or the ratio of tube volume to tube length [28], can lead to aesthetically pleasing ‘ideal’ knots. The method of braid generation (and knot generation via closed braids) described here yields similar results, but operates via a quite different process. Here the topological object grows from initial conditions under the guidance of a Hamiltonian system. With energy minimization, a pre-existing object relaxes to a simpler form by dissipating excess energy.

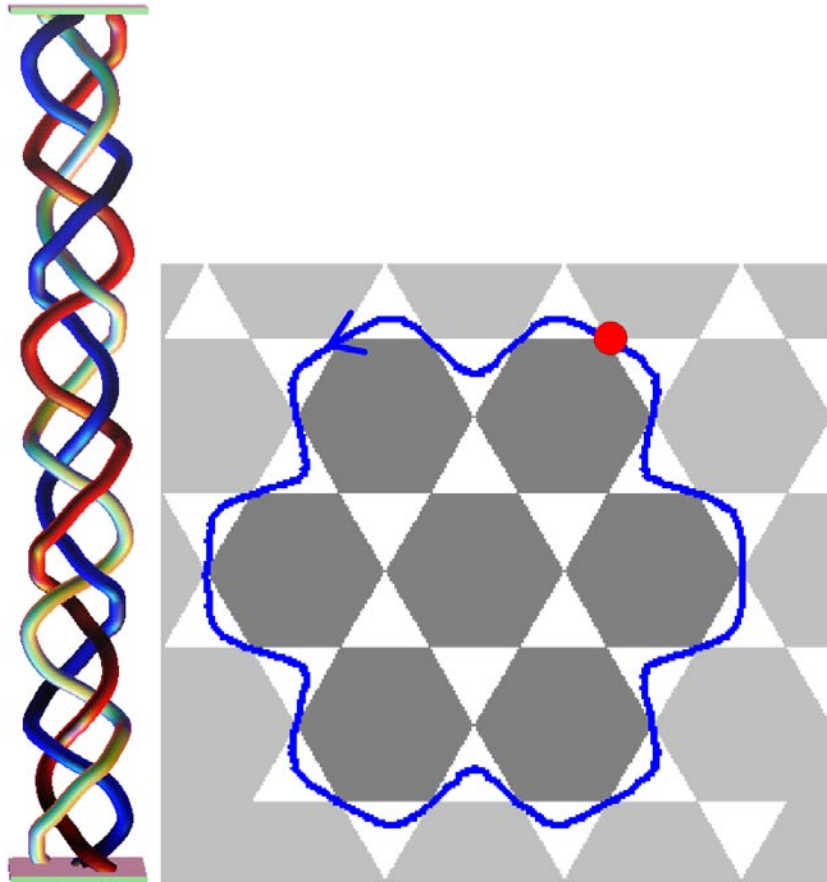


Figure 4. Braid and winding diagram for $\rho = 1$ and $\operatorname{Re} \lambda_{ab}(0) = 0$, $\operatorname{Re} \lambda_{bc}(0) = 0$ and $\operatorname{Re} \lambda_{ca}(0) = -\frac{3}{2}$. For this braid, $\operatorname{Re} \Psi_{abc}(P) = 7$.

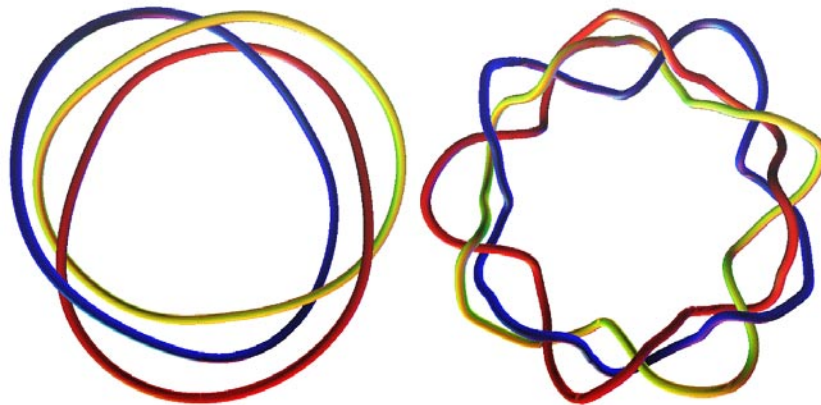


Figure 5. Closed braids associated with figures 2 and 4. The link on the left is an example of the Borromean rings.

Acknowledgments

I am grateful to Yoshi Kimura for useful discussions and help with the numerical code. This paper was partly funded by PPARC grant GR/L63143.

References

- [1] Moore C 1993 Braids in classical dynamics *Phys. Rev. Lett.* **70** 3675
- [2] Clausen S, Helgesen G and Skjeltorp A T 1998 Braid description of collective fluctuations in a few-body system *Phys. Rev. E* **58** 4229
- [3] Boyland P L, Aref H and Stremmer M A 2000 Topological fluid mechanics of stirring *J. Fluid Mech.* **403** 277
- [4] Vassiliev V A 1990 Cohomology of knot spaces *Adv. Sov. Math.* **1** 23
- [5] Birman J S and Lin 1993 Knot polynomials and Vassiliev's invariants *Invent. Math.* **111** 225
- [6] Kontsevich M 1993 Vassiliev's knot invariants *Adv. Sov. Math.* **16** 137
- [7] Chmutov S and Duzhin S 1999 The Kontsevich integral *Preprint*
- [8] Bar-Natan D 2000 Bibliography of Vassiliev invariants, webpage <http://www.ma.huji.ac.il/drorbn>
- [9] Epple M 1998 Orbits of asteroids, a braid, and the first link invariant *Math. Intelligencer* **20** 45
- [10] Cromwell P, Beltrami E and Rampichini M 1998 The Borromean rings *Math. Intelligencer* **20** 53
- [11] Fenn R A 1983 Techniques of geometric topology *London Math. Soc. Lecture Note Series* vol 57 (Cambridge: Cambridge University Press)
- [12] Moffatt H K 1969 The degree of knottedness of tangled vortex lines *J. Fluid Mech.* **35** 117
- [13] Berger M A and Field G B 1984 The topological properties of magnetic helicity *J. Fluid Mech.* **147** 133
- [14] Laurence P and Avellaneda M 1993 A Moffatt–Arnol'd formula for the mutual helicity of linked flux tubes *Geophys. Astrophys. Fluid Dyn.* **69** 243
- [15] Arnold V I and Khesin B A 1998 *Topological Methods in Hydrodynamics* (New York: Springer)
- [16] Monastyrsky M I and Retakh V 1986 Topology of linked defects in condensed matter *Commun. Math. Phys.* **103** 445
- [17] Monastyrsky M I and Sasarov P V 1987 Topological invariants in magnetic hydrodynamics *Sov. Phys.–JETP* **93** 1210
- [18] Berger M A 1990 Third order link integrals *J. Phys. A: Math. Gen.* **23** 2787
- [19] Evans W N and Berger M A 1992 A hierarchy of linking integrals *Topological Aspects of the Dynamics of Fluids and Plasmas (Santa Barbara NATO ASI Proc.)* ed H K Moffatt, G M Zaslavsky, P Comte and M Tabor (Dordrecht: Kluwer) p 237
- [20] Ruzmaikin A and Akhmetiev P 1994 Topological invariants of magnetic fields, and the effect of reconnections *Phys. Plasmas* **1** 331
- [21] Laurence P and Stredulinsky E 2000 Asymptotic Massey products, induced currents and Borromean torus links *J. Math. Phys.* **41** 3170
- [22] Berger M A 1991 Third order braid invariants *J. Phys. A: Math. Gen.* **24** 4027
- [23] Berger M A 1994 Minimum crossing numbers for three-braids *J. Phys. A: Math. Gen.* **27** 6205
- [24] Willerton S 1997 *PhD Thesis* University of Edinburgh
- [25] Aref H, Rott N and Thomann H 1992 Gröbli's solution of the three vortex problem *Annu. Rev. Fluid Mech.* **24** 1
- [26] Moffatt H K 1990 The energy spectrum of knots and links *Nature* **347** 367
- [27] Freedman M H and He Z X 1991 Divergence-free fields—energy and asymptotic crossing number *Ann. Math.* **134** 189
- [28] Katritch V, Bednar J, Michoud D, Scharein R G, Dubochet J and Stasiak A 1996 Geometry and physics of knots *Nature* **384** 142